J. Fluid Mech. (1987), *vol.* 176, *pp.* 265–281
Printed in Great Britain

Temperature-dissipation measurements in a turbulent boundary layer

By L. V. KRISHNAMOORTHY AND R. A. ANTONIA
Department of Mechanical Engineering, University of Newcastle, NSW 2308, Australia

(Received 28 August 1985 and revised form 27 May 1986)

The three components of the average temperature dissipation have been measured using a pair of parallel cold wires in an approximately self-preserving turbulent boundary layer. The mean square value of $\theta_{,x}$, the temperature derivative in the longitudinal direction, is determined mainly by the use of Taylor's hypothesis, following direct verification of this hypothesis at a few locations in the flow. Mean square values of $\theta_{,y}$ and $\theta_{,z}$, the temperature derivatives in directions normal to the flow, were estimated mainly from the curvature of spatial temperature autocorrelations. In the outer layer, the measurements indicate that $\overline{\theta^2_{,z}} > \overline{\theta^2_{,y}} > \overline{\theta^2_{,x}}$, and the resulting distribution for dissipation leads to a good closure of the $\frac{1}{2}\overline{\theta^2}$ budget. In the near-wall region the measurements indicate that $\overline{\theta^2_{,y}} > \overline{\theta^2_{,z}} > \overline{\theta^2_{,x}}$. The ratios $\overline{\theta^2_{,y}}/\overline{\theta^2_{,x}}$ and $\overline{\theta^2_{,z}}/\overline{\theta^2_{,x}}$ are as large as 13 and 7 respectively at $y^+ = 12$, underlining the strong anisotropy in this region. The behaviour of the turbulent diffusion, estimated by difference, provides reasonable support for the accuracy of the near-wall temperature-dissipation measurements. Using existing data of near-wall distributions of the turbulent energy and of its dissipation rate, the timescale for the turbulent-energy dissipation is found to be approximately equal to that for the temperature dissipation.

1. Introduction

There have been numerous attempts at obtaining turbulence models for the numerical calculation of the velocity field of a turbulent boundary layer. Two such models are the 'k–ϵ' method and the second-order model. In the first of these (Launder & Spalding 1974), transport equations for the turbulent kinetic energy ($\equiv \frac{1}{2}\overline{q^2}$, where $\overline{q^2} = \overline{u^2}+\overline{v^2}+\overline{w^2}$) and $\bar{\epsilon}$, the average dissipation of the kinetic energy, are constructed but the model is of the eddy-viscosity type, the magnitude of the effective eddy viscosity being set by the calculated values of $\overline{q^2}$ and $\bar{\epsilon}$. In second-order models, the second-moment correlations representing the turbulent transport of momentum or heat are obtained directly from their own transport equations. Shih & Lumley (1986) have developed a second-order model of near-wall turbulence and used it to calculate, *inter alia*, $\overline{u^2}, \overline{v^2}, \overline{w^2}$ and $\bar{\epsilon}$ in a zero-pressure-gradient boundary layer.

The extension of these models to the heat transfer case has received somewhat less attention perhaps because, as Launder (1976) points out, the correct calculation of the velocity field is an essential prerequisite to the temperature calculation. It is reasonable to suggest however that more accuracy can be achieved when modelling terms in a temperature-field calculation than for a velocity-field computation. For example, in analogy to the 'k–ϵ' approach, transport equations can be written for $\frac{1}{2}\overline{\theta^2}$, where $\overline{\theta^2}$ is the temperature variance and $\bar{\epsilon}_\theta$, the average dissipation of $\frac{1}{2}\overline{\theta^2}$. The pressure fluctuation does no appear in the equation for $\frac{1}{2}\overline{\theta^2}$ and all the terms of this

equation are, in principle, measurable. Similarly, the transport equation for $\bar{\epsilon}_\theta$ is less daunting both from modelling and measurement viewpoints, than that for $\bar{\epsilon}$ (e.g. Launder 1976; Antonia & Browne 1983). It should also be noted that, regardless of whether a 'k–ϵ' model or a second-order model is used, the timescales $\tau_u (\equiv \overline{q^2}/\bar{\epsilon})$ and $\tau_\theta (\equiv \overline{\theta^2}/\bar{\epsilon}_\theta)$ play important roles in the modelling. Since all the terms in $\bar{\epsilon}_\theta$ can be measured, the temperature timescale can be determined, thus obviating the need to assume isotropy, as is often done when the velocity timescale is obtained.

In the present paper we focus our attention on the measurement of $\bar{\epsilon}_\theta$ throughout the boundary layer but especially in the near-wall region ($y^+ \lesssim 30$, where the superscript denotes normalization by the friction velocity u_τ and the kinematic viscosity ν). Apart from being an important flow region, there is evidence (Launder 1984) that an abandonment of the wall-function approach may lead to an improvement in calculating momentum and scalar transports in the immediate wall region. There are few measurements of all three components of the average temperature dissipation $\bar{\epsilon}_\theta$ in a turbulent boundary layer and, to our knowledge, no measurements in the immediate vicinity of the wall. The average dissipation $\bar{\epsilon}_\theta$ is defined by

$$\bar{\epsilon}_\theta = \alpha(\overline{\theta_{,x}^2} + \overline{\theta_{,y}^2} + \overline{\theta_{,z}^2}), \tag{1}$$

where α is the thermal diffusivity, $\theta_{,x} \equiv \partial\theta/\partial x$, x and z are in the longitudinal and spanwise directions respectively, y is in the direction normal to the wall. Simultaneous measurements of the three components of $\bar{\epsilon}_\theta$ were made in the logarithmic region by Sreenivasan, Antonia & Danh (1977) using two pairs of cold wires with fixed separations in the y- and z-directions. The size of this four-wire probe precluded measurements being made very close to the wall. Verollet (1972) obtained the three components of $\bar{\epsilon}_\theta$ using two-point-temperature-autocorrelation functions in the region $y^+ \gtrsim 30$. In the previous two studies, the thermal layer developed within a nearly self-preserving velocity boundary layer. The main aim of the present investigation is to determine the behaviour of $\bar{\epsilon}_\theta$ in the region $y^+ \lesssim 30$ as accurately as possible with a view to providing useful data for turbulence modelling. Another aim is to quantify the departure of the temperature dissipation from local isotropy in the near-wall region.

The present measurements of $\bar{\epsilon}_\theta$ are made in a boundary layer with approximately the same origins for velocity and temperature fields. Details of the experiment are given in §2 and the various methods used to estimate $\bar{\epsilon}_\theta$ are presented in §3. A discussion of how $\bar{\epsilon}_\theta$ and its components are distributed across the layer is given in §4. The accuracy of $\bar{\epsilon}_\theta$ in the outer layer is considered in §5 by examining the balance in the completely measured budget of $\frac{1}{2}\overline{\theta^2}$. The accuracy of $\bar{\epsilon}_\theta$ in the near-wall region is indirectly checked in §6 by considering the behaviour of the turbulent diffusion which is inferred by difference. The distribution of the temperature timescale is discussed in §7.

2. Experimental arrangement

The suction-type wind tunnel used in the present investigation has a rectangular working section of 60 × 12 cm and a length of 1.8 m. The boundary layer develops over the aluminium floor (1.27 cm thick) of this section which can be heated using twelve Sierracin pads (0.1 mm thick) connected in series and arranged into two rows of six along the length of the section. These pads are bonded to the bottom of the aluminium plate and thermal insulation (45 mm thick) ensures that the heat loss from the back of the plate is small. All the pads are a.c. heated using a transformer operated

at 125 V and 8 A. Approximately one hour of tunnel running time is required to establish stable conditions. The plate temperature is continuously monitored using integrated-circuit temperature transducers located in small holes (5 mm diameter, 3.8 mm deep) drilled in the back of the aluminium plate. These transducers are held in position using a highly conductive silicone compound (Unick UH-102). When a constant current is maintained through the transistor junctions of the transducer, the output is proportional to the absolute temperature.

Measurements were made at a free-stream velocity (U_1) of 9 ms^{-1} and the difference ($T_w - T_1$) between the wall and the free-stream temperature was approximately 9.6 K. The boundary layer was tripped using a 1.5 mm diameter rod placed on the floor of the working section, at $x = 7$ mm, where x is measured from the beginning of the test section. At $x = 1.4$ m, the boundary-layer thickness δ, defined as the distance from the wall where $\bar{U} = 0.995U_1$, and the thermal layer thickness δ_T, defined as the distance from the wall where $(T_w - \bar{T}) \approx 0.995(T_w - T_1)$, were approximately the same, equal to 28 mm. The friction velocity u_τ [$= (\tau_w/\rho)^{\frac{1}{2}}$, τ_w is the wall shear stress, ρ is the density] and the friction temperature $\theta_\tau (= Q_w/\rho_{c_p} u_\tau$, Q_w is the wall heat flux, c_p is the specific heat at constant pressure) were equal to 0.38 ms^{-1} and 0.42 K respectively. The Reynolds number $U_1\delta_2/\nu$ based on the momentum thickness δ_2 is about 2000. The enthalpy thickness

$$\delta_i \left\{ = \int_0^\delta \left[\frac{(\bar{U}/U_1)(\bar{T} - T_1)}{(T_w - T_1)} \right] \mathrm{d}y \right\}$$

is 3.4 mm. Since the walls of the working section are parallel, the boundary layer develops in a favourable pressure gradient. The magnitude $(\nu/u_\tau^3)(\mathrm{d}p/\mathrm{d}x)$ of this pressure gradient was -10^{-3}, over approximately the last two-thirds of the working-section length.

The temperature autocorrelation function, for zero time delay,

$$\rho_\beta = \frac{\overline{\theta(\beta)\,\theta(\beta + \Delta\beta)}}{\overline{\theta^2(\beta)}^{\frac{1}{2}}\,\overline{\theta^2(\beta + \Delta\beta)}^{\frac{1}{2}}}, \tag{2}$$

where β ($\equiv x, y, z$) denotes the position and $\Delta\beta$, the separation, was obtained with a pair of cold wires mounted on separate traversing units. One of the units provided displacements in all three directions while the other allowed displacement only in the y-direction. The displacements were read on dial gauges with a least count of 0.01 mm. The cold wires (Pt–10% Rh) of 0.63 μm diameter were aligned in the z-direction and had a length of about 0.50 mm. They were operated with in-house constant-current circuits. The combination of a small value (0.1 mA) for the current and the chosen experimental conditions resulted in only a small velocity sensitivity of the cold wires. This sensitivity was estimated using an approach similar to that outlined by Wyngaard (1971). At $y^+ = 2$, the error in $\overline{\theta^2}_{,x}$ due to this contamination was about 0.01%. The temperature coefficient of resistivity of the 0.63 μm (Pt–10% Rh) wire was found to be 0.0016 K^{-1} (±5%) by calibrating the wire against a platinum resistance thermometer (least count = 0.01 K) in the core of a plane jet. Wire resistances were matched, during etching, to within ±7%. The initial separation, in the y-direction, between the wires placed in the air stream was measured using a cathetometer with a least count of 0.01 mm. Subsequent separations were determined using the dial gauge on the traversing unit. The reproducibility of the initial separation was established, by repeating measurements, to be ±0.03 mm.

The mean temperature was inferred from the d.c. output of the constant-current

circuit with a TSI 1076 voltmeter. The signals from the two cold wires were passed through buck and gain units to offset the d.c. components and provide suitable amplification to enable the signals to be recorded on an FM tape (HP3968A) at 381 mm/s. The output voltages from the buck and gain units were differentiated with an analogue circuit designed to have unity gain at 1 kHz. The differentiated signals were also recorded. The signals were low-pass filtered (Krohn–Hite model 3322) before digitizing on a PDP 11/34 computer. The filter settings for the differentiated signals were determined during the course of the experiments, using a procedure similar to that outlined in Antonia, Satyaprakash & Hussain (1980). The spectrum of the signal at the output of the buck and gain unit was displayed on the built-in oscilloscope of a two-channel real-time spectrum analyser (HP3582A). The frequency at which this spectrum merged into the noise spectrum (obtained and stored in the spectrum analyser at the beginning of the experiment when the wires were in the free stream) was used as the cutoff frequency. The low-pass filter settings (f_c) used for determining ρ_β, varied from 0.5 kHz (at $y^+ = 2$) to 2 kHz (at $y^+ = 540$). The sampling frequency, f_s, equal to $2f_c$, was in the range $0.4f_K$ to $0.7f_K$, where f_K is the Kolmogorov frequency. The shape of ρ_β was not affected by the precise value of f_s. The magnitude of ρ_β was only marginally affected: for example, a reduction of about 0.5 % occurred when f_s was increased from $0.2f_K$ to $2.0f_K$. The 40 s duration of the digital records was sufficient for ρ_β to converge to within ± 0.5 % of its final value.

Velocity fluctuations u and v, in the x- and y-directions respectively, were measured at the same time as the temperature fluctuation θ with an X-probe/cold-wire arrangement. The hot wires of the X-probe (5 μm diameter, Pt–10 % Rh, 1 mm length) were mounted in the (x, y)-plane with a separation of about 1 mm in the z-direction. The hot wires were operated with DISA 55M10 constant temperature anemometers at a resistance ratio of 1.8. A 0.63 μm cold wire (Pt–10 % Rh) was located 0.7 mm upstream of the geometrical centre of the X-probe and orthogonally to the (x, y)-plane. The possible interference of the unetched wire stubs with the X-probe was avoided by the use of a 1.1 mm long cold wire. The signals from the X-wire and cold wire were passed through in-house buck and gain units and recorded on an analogue tape recorder before digitizing into a PDP 11/34 computer. The signals were low-pass filtered before digitizing at $f_s = 5$ kHz.

To account for the temperature sensitivity of hot wires, each instantaneous data point was corrected using the following relationship

$$E^2 \frac{(T_p - T_1)}{(T_p - T)} = A + BU^n, \tag{3}$$

where A, B, n are the calibration constants in the free stream (temperature T_1), T_p is the hot-wire temperature and T the instantaneous fluid temperature. The hot-wire voltage time series was then converted into time series for u and v using the yaw calibration curve. The resulting distributions of Reynolds shear stresses agreed to within ± 2 % with those obtained when the wall was not heated, thus supporting the assumption that temperature was a passive marker of the flow.

3. Different methods for determining the components of $\bar{\epsilon}_\theta$

Since it was important to establish the accuracy of $\overline{\theta^2}_{,x}, \overline{\theta^2}_{,y}, \overline{\theta^2}_{,z}$, several methods were used for their determination. In particular, $\overline{\theta^2}_{,x}$ was determined by two different methods:

(i) from the two-point temperature autocorrelation using either the approach of Rose (1966) or by fitting an osculating parabola to the correlation near the origin;

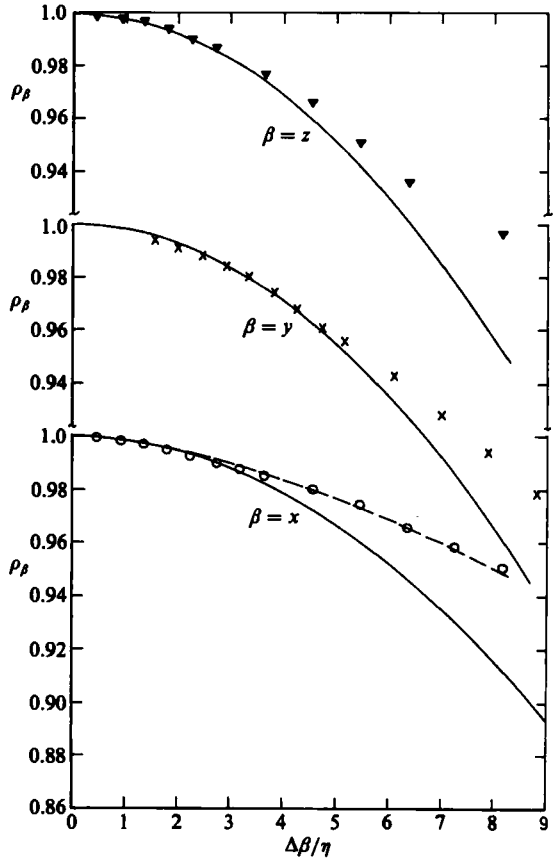

FIGURE 1. Temperature autocorrelation coefficients as a function of the separation $\Delta\beta/\eta$ at $y^+ = 180$. ○, $\beta = x$; ×, y; ▼, z; ---, least-squares fits to the data; ——, equation (6).

(ii) from the time derivative of θ using Taylor's hypothesis; the hypothesis was checked by forming the difference between the cold-wire signals over a range of streamwise separation.

(i) The variance $\overline{\theta^2}_{,x}$ was first determined by the approach used by Rose (1966). Using a Taylor series expansion for ρ_x and assuming homogeneity, ρ_x can be approximated, for small values of Δx, by (e.g. Hinze 1959)

$$\lim_{\Delta x \to 0} \rho_x \simeq 1 - \frac{(\Delta x)^2}{\lambda_x^2}, \tag{4}$$

to order $(\Delta x)^4$. In (4), λ_x is the longitudinal Taylor microscale for temperature

$$\lambda_x = \left(2\frac{\overline{\theta^2}}{\overline{\theta^2}_{,x}}\right)^{\frac{1}{2}}. \tag{5}$$

The correlation ρ_x, obtained at $y^+ = 180$, is shown in figure 1 as a function of $\Delta x/\eta$, where η is the Kolmogorov lengthscale ($\equiv \nu^{\frac{3}{4}}/\bar{\epsilon}^{\frac{1}{4}}$, where $\bar{\epsilon}$ is the average turbulent-energy dissipation determined by assuming local isotropy and the mean-square value of the derivative of the longitudinal velocity fluctuation u). The quantity $(1-\rho_x)$ is plotted in figure 2 as a function of $\Delta x/\eta$. The intersection of the line of slope +2 with the $(1-\rho_x)$-axis yields values of 27.7 for λ_x/η and 0.07 K²/mm² for $\overline{\theta^2}_{,x}$. The

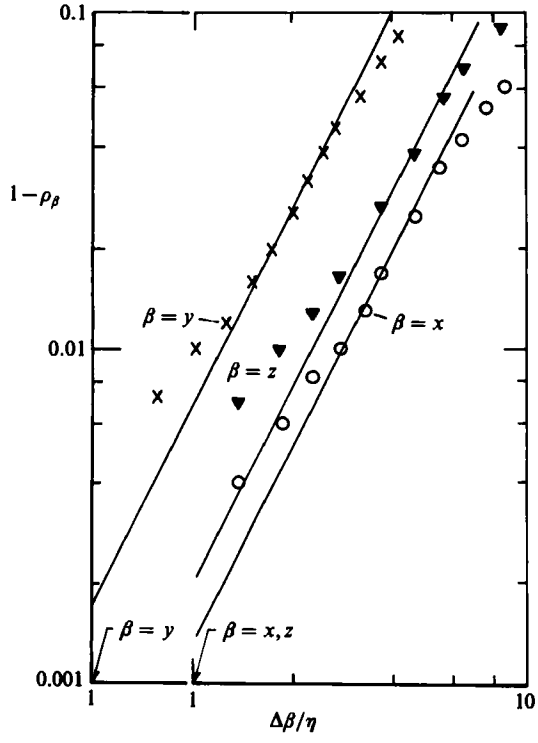

FIGURE 2. Log–log representation of $(1-\rho_\beta)$ as a function of the separation $\Delta\beta/\eta$ at $y^+ = 180$. Symbols are as in figure 1. ——, lines of best fit with a slope of +2. Note the shift in origin for the abscissa.

corresponding turbulence Reynolds number $(\lambda_x \overline{u^2}^{\frac{1}{2}}/\nu)$ is 120. Although the accuracy of (4) increases as Δx decreases, the data in figure 2 deviate from the line of slope +2 at very small separations. Similar departures were also observed by Rose (1966) and Antonia *et al.* (1984). These departures are due to an increase in the experimental uncertainty as ρ_x exceeds 0.98 for the first three data points (smallest $\Delta x/\eta$) in figure 2.

Another estimate of λ_x was obtained from the curvature of the osculating parabola to ρ_x for small values of Δx, viz.

$$\lambda_x = \left(\frac{-2}{[\partial^2\rho_x/\partial(\Delta x)^2]_{\Delta x \to 0}}\right)^{\frac{1}{2}}. \tag{6}$$

The broken line in figure 1 represents a cubic-spline least-squares fit to the data. The fit, implemented by computer, was made to satisfy $\partial\rho_x/\partial(\Delta x)$ at $\Delta x = 0$ by reflecting the first few points about the origin. Symmetry of ρ_x with respect to Δx is a consequence of the approximate streamwise homogeneity of the flow and was verified directly by measurement at a few values of x. The second derivative was obtained by numerically differentiating the best fit to ρ_x, for which $\lambda_x/\eta = 28$. The corresponding osculating parabola is shown in figure 1. The value of $\overline{\theta^2}_x$ obtained from (6), was within 2 % of the value obtained using (4). This close agreement is only an internal consistency check of the data reduction since (4) and (6) are equivalent.

(ii) The microscale λ_x was obtained from the time derivative of θ and Taylor's hypothesis $(\partial/\partial x = -\bar{U}^{-1}\,\partial/\partial t)$. The experiments of Antonia *et al.* (1984) have provided a direct check of this hypothesis on the centreline of a plane jet. A procedure similar to that of Antonia *et al.* was used to verify the hypothesis in the present flow.

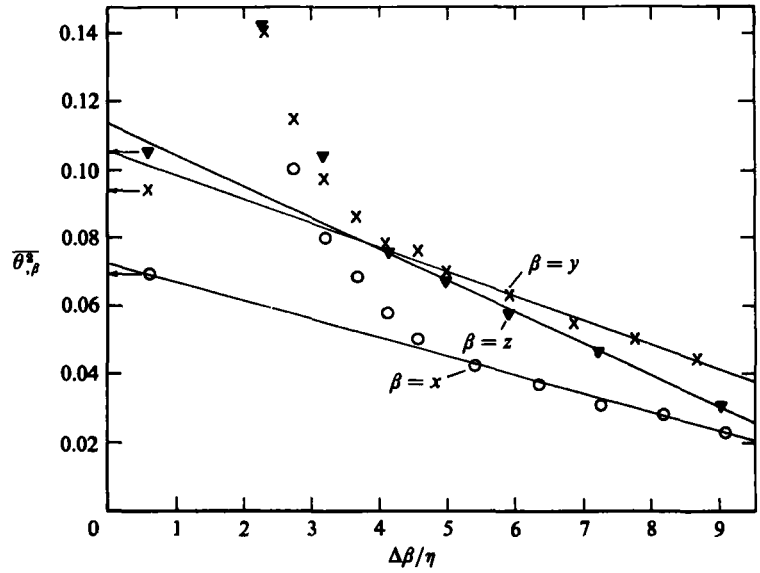

FIGURE 3. Finite-difference approximation to $\overline{\theta^2_{,\beta}}$ as a function of the separation $\Delta\beta/\eta$ at $y^+ = 180$. Symbols are as in figure 1. ——, lines of best fit for $5 \leqslant \Delta\beta/\eta \leqslant 9$. Arrows indicate values obtained with (6).

An average value for $\overline{(\partial\theta/\partial t)^2}$ of 4.2 $\mathrm{K^2\ s^{-2}}$, with a standard deviation of 4%, was first estimated by repeating the experiment 13 times. Using Taylor's hypothesis, with $\overline{U} = 7.5\ \mathrm{ms^{-1}}$, $\overline{\theta^2_{,x}}$ was equal to 0.075 $\mathrm{K^2/mm^2}$ and the corresponding value for λ_x was within 4% of the value obtained by method (i).

A more direct estimate of $\overline{\theta^2_{,x}}$ was then inferred from the difference $\Delta\theta$ between two temperature signals separated in the x-direction, using the approximation $\theta_{,x} = \Delta\theta/\Delta x$ for sufficiently small values of Δx. When Δx is too small ($\Delta x/\eta \lesssim 4$), a reliable estimate of $\theta_{,x}$ is difficult because of the systematic errors due to uncertainties in estimating the temperature sensitivity of the wires (Mestayer & Chambaud 1979; Browne, Antonia & Rajagopalan 1983*b*). Although we do not have data for $\Delta x/\eta > 10$, we would expect $\overline{\theta^2_{,x}}$ to decrease more rapidly in this range (as observed for example, by Browne, Antonia & Chambers 1983*a*) than over the range $4 \leqslant \Delta x/\eta \leqslant 10$.

The difference $\Delta\theta$ was formed on a computer for a number of separations. The quantity $\overline{(\Delta\theta/\Delta x)^2} = \overline{\theta^2_{,x}}$ is plotted in figure 3 *vs.* $\Delta x/\eta$. A linear extrapolation to zero separation was carried out in the manner outlined by Browne *et al.* (1983*a*) for data in the range $5 \leqslant \Delta x/\eta \leqslant 9$. This resulted in a value of 0.077 $\mathrm{K^2/mm^2}$ for $\overline{\theta^2_{,x}}$. This value and that obtained by method (i) were within ± 7% of the value obtained using Taylor's hypothesis. Since this agreement was found to apply, with approximately the same bounds of uncertainty at other values of y^+ (5, 30, 60 and 120), Taylor's hypothesis was used to obtain $\overline{\theta^2_{,x}}$ at every location in the flow.

Estimates of $\overline{\theta^2_{,y}}$ and $\overline{\theta^2_{,z}}$ were made at $y^+ = 180$ via the correlation method and the finite-difference approximation (figures 1, 2 and 3). Agreement between the two methods (table 1) was within 12% for $\overline{\theta^2_{,y}}$ and $\overline{\theta^2_{,z}}$. As the extrapolation to zero separation in method (ii) is relatively inaccurate (Browne *et al.* 1983*a*), the correlation method was preferred in determining $\overline{\theta^2_{,y}}$ and $\overline{\theta^2_{,z}}$.

In the near-wall region, the estimation of $\overline{\theta^2_{,y}}$ via equations analogous to (4) and (6) would be grossly inaccurate because of the inadequacy of the homogeneity in the

Method	$\overline{\theta^2}_{,x}$	$\overline{\theta^2}_{,y}$	$\overline{\theta^2}_{,z}$
		K^2/mm^2	
(i) (a) Correlation	0.069	0.094	0.105
(b) Method of Rose (1966)	0.070	0.096	0.107
(ii) (a) Finite difference	0.077	0.105	0.116
(b) Taylor's hypothesis	0.075	—	—

TABLE 1. Comparison of different estimates of $\overline{\theta^2}_{,\beta}$

y-direction. To take into account the effect of relatively large gradients, in this direction, of $\overline{\theta^2}$, approximations, such as (4) and (6), require modification. An appropriate starting point is the Taylor series expansion

$$\theta(y+\Delta y) = \theta(y)+\Delta y\left(\frac{\partial\theta(y)}{\partial y}\right)_{\Delta y=0}+\tfrac{1}{2}(\Delta y)^2\left(\frac{\partial^2\theta(y)}{\partial y^2}\right)_{\Delta y=0}, \tag{7}$$

to order $(\Delta y)^3$. Using (7) and averaging with respect to time, expressions can be obtained for $\overline{\theta(y+\Delta y)\theta(y)}$ and $\overline{[\theta(y+\Delta y)]^2}$. An expression for the autocorrelation function ρ_y can then be written†, using definition (2) as

$$\rho_y = 1-\tfrac{1}{2}(\Delta y)^2\left\{\frac{\overline{\theta^2}_{,y}}{\overline{\theta^2}}-\frac{1}{4\overline{\theta^2}^2}\left(\frac{\partial\overline{\theta^2}}{\partial y}\right)^2\right\}, \tag{8}$$

to order $(\Delta y)^3$. The second term inside the brackets becomes small ($< 10\%$) in comparison to the first term at $y^+ = 9$, so that $\overline{\theta^2}_{,y}$ can be estimated with sufficient accuracy using expressions similar to (4) and (6) in the region $y^+ \geqslant 9$. To determine $\overline{\theta^2}_{,y}$ for $y^+ < 9$, (8) was applied at each value of Δy. The magnitude of $\partial\overline{\theta^2}/\partial y$ was estimated, at $\frac{1}{2}\Delta y$, by numerically differentiating a best fit to the $\overline{\theta^2}$ measurements. The resulting values of $\overline{\theta^2}_{,y}$, calculated using (8), are approximately constant over a small range of Δy. The estimate of $\overline{\theta^2}_{,y}$ at $y^+ = 5$, using (8) is shown in figure 4.

4. Variation of $\overline{\theta^2}_{,x}$, $\overline{\theta^2}_{,y}$ and $\overline{\theta^2}_{,z}$

Distributions of $\overline{\theta^2}_{,x}$, $\overline{\theta^2}_{,y}$, $\overline{\theta^2}_{,z}$, normalized using δ and the friction temperature θ_τ are shown in figure 5 as a function of y^+ or y/δ. The error bars in figure 5 represent the uncertainties in the three components of dissipation. The large uncertainty in $\overline{\theta^2}_{,y}$ for $y^+ \leqslant 20$, is mainly associated with the determination of the initial separation $\Delta y^+ (\approx 1)$. Further, the maximum correlation obtained was not quite unity ($\rho_\beta = 0.980$) due to the contamination of the signal by electronic noise. A correction based on the r.m.s. values of the signals and the correlation between the noise components in different circuits, was applied to the measured correlation, thereby increasing the magnitude of ρ_β to almost unity (typically in excess of 0.99).

The three components of $\bar{\epsilon}_\theta$ in the region $y^+ \geqslant 180$ follow the inequality $\overline{\theta^2}_{,z} > \overline{\theta^2}_{,y} > \overline{\theta^2}_{,x}$. In particular, the relative magnitudes of these quantities are similar to those obtained by Sreenivasan, Antonia & Danh (1977). Defining $K_1 = \overline{\theta^2}_{,y}/\overline{\theta^2}_{,x}$ and $K_2 = \overline{\theta^2}_{,z}/\overline{\theta^2}_{,x}$, Sreenivasan *et al.* obtained average values of K_1 and K_2 equal to about 1.2 and 1.5 respectively. The present average values of K_1 and K_2 are 1.4 and 1.6 respectively. For $30 \leqslant y^+ \leqslant 180$, the present distributions are qualitatively similar

† A similar expression was used by Townsend (1956) for the correlation between $u(y)$ and $u(y+\Delta y)$ in the near-wall region.

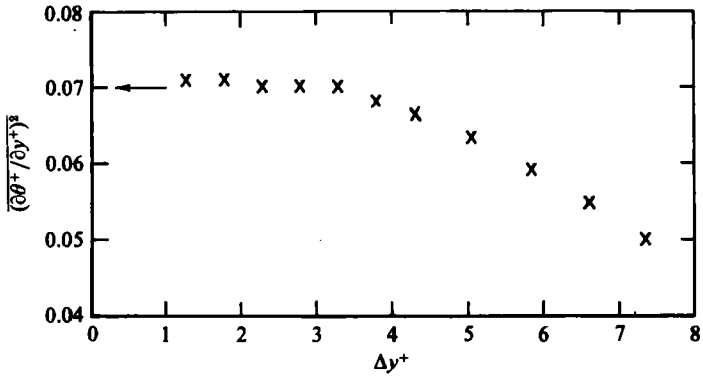

FIGURE 4. Non-dimensional finite-difference approximation to $\overline{\theta^2}_{,y}$ in the near-wall region as a function of Δy^+. ×, $y^+ = 5$. Arrow shows value at zero separation.

to those of Verollet (1972). Since K_1 and K_2 are both greater than unity, $\overline{\theta^2}_{,y} > \overline{\theta^2}_{,z} > \overline{\theta^2}_{,x}$. The present values of K_1 and K_2 varied from 1.2 and 1.4 at $y^+ = 180$ to 5 and 4 respectively at $y^+ = 30$. Verollet's values of K_1 and K_2 increased from 1 at $y^+ \approx 180$ to about 2.5 and 2 respectively at $y^+ \approx 30$. In the region $y^+ < 30$, $\overline{\theta^2}_{,y} > \overline{\theta^2}_{,z} > \overline{\theta^2}_{,x}$. A plausible qualitative explanation for the relative magnitudes of $\overline{\theta^2}_{,x}, \overline{\theta^2}_{,y}, \overline{\theta^2}_{,z}$ in the near-wall region is provided by an order-of-magnitude argument. If it is assumed that $\overline{\theta^2}_{,\beta}$ is of order $\overline{\theta_0^2}/\lambda_\beta^2$ where θ_0 is a suitable temperature scale and λ_β is a Taylor microscale (Tennekes & Lumley 1972), the attenuating effect of the wall would be such as to affect λ_y more than λ_z or λ_x. One would expect λ_x to be least affected while λ_y should be significantly reduced. In this context, the inequality $\lambda_y < \lambda_z < \lambda_x$ appears reasonable.

The above inequality reflects, at least qualitatively, relative differences in the lengthscales of near-wall flow structures, which can be inferred primarily from available flow visualizations in this flow region. It is well established that the average spanwise wavelength of low-speed streaks is about 100 wall units (e.g. Smith & Metzler 1983). The average streamwise length of these streaks is of the order of 1000 wall units. In his review, Cantwell (1981) reported an average value of 15 wall units for the distance from the wall to the centre of a streamwise vortex. The flow-visualization experiments of Iritani, Kasagi & Hirata (1985) have shown a close similarity between the structures of the thermal fields and momentum fields in the near-wall region. In particular, high-temperature streaks were found to coincide with low-speed streaks whereas low-temperature streaks corresponded with high-speed streaks. The present values of K_1 and K_2 are in the range 9–85 and 2–7 respectively over the near-wall region, underlining the strong anisotropy of this region. This anisotropy is broadly similar to that observed for some of the measurable components of turbulent-energy dissipation. For example, Klebanoff (1954) found that the ratio $\overline{u^2}_{,y}/\overline{u^2}_{,x}$ is equal to $\overline{u^2}_{,z}/\overline{u^2}_{,x}$ and is as high as 10 at $y^+ \approx 14$ ($y/\delta = 0.005$).

The measured value of $\overline{\theta^2}_{,x}$ should be reduced due to the attenuation of the high-frequency part of the derivative spectrum resulting from the finite length of the cold wire. Wyngaard's (1971) correction for the attenuation of the temperature dissipation assumes isotropy and the Corrsin–Pao form of the three-dimensional temperature spectrum. This analysis indicates that the present values of $\overline{\theta^2}_{,x}$ (for the 0.50 mm long cold wire, $l/\eta \approx 4.55$, where η is the Kolmogorov microscale at $y^+ = 180$) are underestimated by 30 % at $y^+ = 5$ and 13 % at $y^+ = 540$. Since the analysis gives only an approximate indication of the attenuation, $\overline{\theta^2}_{,x}$ was re-measured

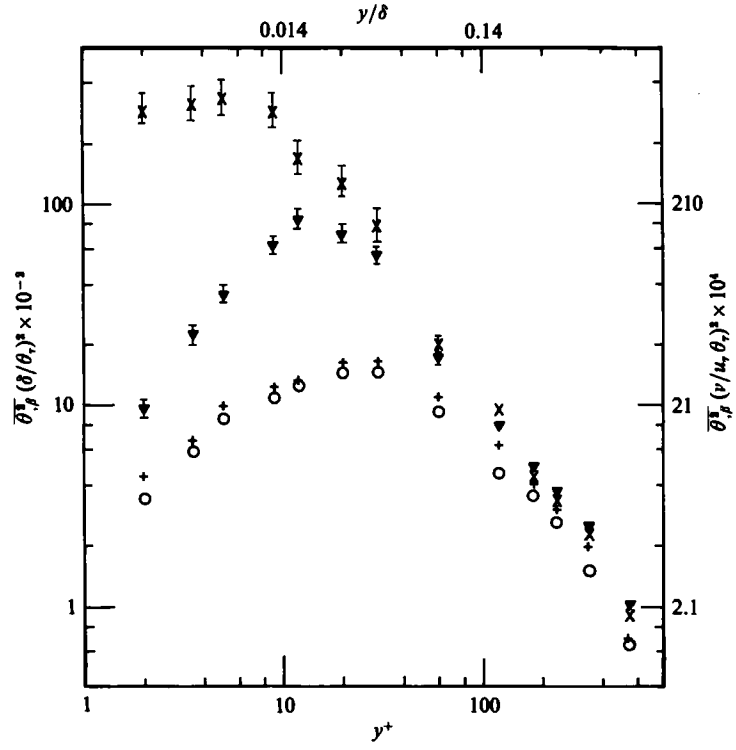

FIGURE 5. Distributions of mean-square values of temperature derivatives across the boundary layer. Symbols are as in figure 1. $l/\eta = 4.55$. +, $\overline{\theta^2_{,x}}$ ($l/\eta = 1.82$).[, error bars (see text).

with a shorter wire ($l/\eta = 1.8$). The measured increase in $\overline{\theta^2_{,x}}$ due to the reduction in l/η agreed, to within $\pm 8\%$, with that predicted by Wyngaard's analysis. The reduction in l also brings about a reduction in l/d and one should strictly take into account a possible decrease in $\overline{\theta^2_{,x}}$ due to increasing end-conduction effects (e.g. Lecordier *et al.* 1984). Since the contribution of $\overline{\theta^2_{,x}}$ to $\bar{\epsilon}_\theta$ is very small in the near-wall region (2.5% at $y^+ = 5$ and 25% for $y^+ \geqslant 180$), we chose to neglect possible end-conduction errors, and consistently used values of $\overline{\theta^2_{,x}}$ which were obtained with the shorter wire ($l/\eta = 1.8$). Because the measured spectra of $\theta_{,y}$ and $\theta_{,z}$ receive most of their contribution from the low-frequency part of the spectrum (e.g. Sreenivasan *et al.* 1977) we have assumed that there is negligible attenuation of $\overline{\theta^2_{,y}}$ and $\overline{\theta^2_{,z}}$ due to wire length.

5. Budget of $\frac{1}{2}\overline{\theta^2}$ in the outer layer

The accuracy of $\bar{\epsilon}_\theta$ in the outer layer ($y^+ \gtrsim 180$, $y/\delta \gtrsim 0.25$) was checked by measuring the remaining terms of the budget of $\frac{1}{2}\overline{\theta^2}$ and by examining the magnitude of the resulting imbalance. The transport equation for $\frac{1}{2}\overline{\theta^2}$ in a two-dimensional flow is (e.g. Corrsin 1953)

$$\underbrace{\tfrac{1}{2}\overline{U}\frac{\partial\overline{\theta^2}}{\partial x}+\tfrac{1}{2}\overline{V}\frac{\partial\overline{\theta^2}}{\partial y}}_{\text{advection 1}}+\underbrace{\overline{u\theta}\frac{\partial\overline{T}}{\partial x}+\overline{v\theta}\frac{\partial\overline{T}}{\partial y}}_{\text{production 2}}+\underbrace{\frac{1}{2}\frac{\partial}{\partial x}(\overline{u\theta^2})+\frac{1}{2}\frac{\partial}{\partial y}(\overline{v\theta^2})}_{\text{turbulent diffusion 3}}-\underbrace{\tfrac{1}{2}\alpha\frac{\partial^2\overline{\theta^2}}{\partial x^2}-\tfrac{1}{2}\alpha\frac{\partial^2\overline{\theta^2}}{\partial y^2}}_{\text{molecular gradient diffusion 4}}+\underbrace{\bar{\epsilon}_\theta}_{\text{dissipation 5}}=0. \quad (9)$$

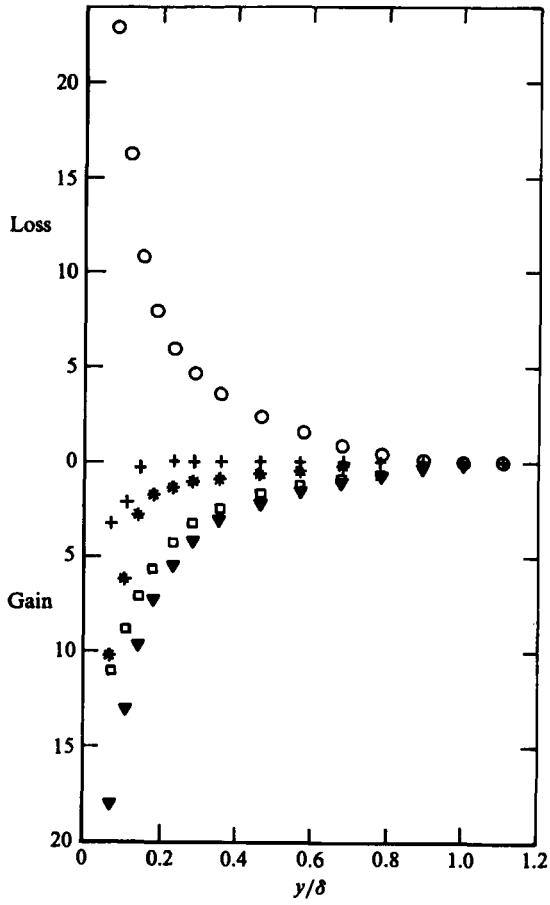

FIGURE 6. Production, dissipation and imbalance of $\frac{1}{2}\overline{\theta^2}$ in the outer layer. All terms are normalized by $(\delta/U_\tau\theta_\tau^2)$. ○, production; ▼, total dissipation; □, isotropic dissipation; +, imbalance for total dissipation; *, imbalance for isotropic dissipation.

The first terms within groupings 2, 3 and 4 were found to be small and have been ignored. The distributions of other terms in (9), made dimensionless by multiplying by $\delta/(u_\tau\theta_\tau^2)$, are shown in figures 6 and 7 in terms of y/δ. Terms 1, 2 and 4 are estimated from least-squares fits to measurements of $\overline{U}/u_\tau$, $\overline{\theta^2}/\theta_\tau^2$ and $\overline{T}/\theta_\tau$. The fits were differentiated numerically and further fits were subsequently applied to the derivative data. The normal velocity $\overline{V}$ was calculated using the continuity equation. Measured values of the (thermometric) heat flux $\overline{v\theta}$ and the product $\overline{v\theta^2}$ were used for terms 2 and 3.

It is clear from figures 6 and 7 that the production and dissipation (figure 6) are nearly equal for $y/\delta > 0.25$ and that advection and turbulent diffusion (figure 7) are approximately in balance for $y/\delta > 0.6$. The isotropic dissipation $(\bar{\epsilon}_\theta)_{\rm iso} = 3\overline{\theta^2}_{,x}$, is also plotted in figure 6. The total dissipation is larger than the isotropic dissipation by an amount varying from 25% at $y/\delta = 0.7$ to 40% at $y/\delta = 0.1$.

The imbalance in the region $y/\delta > 0.25$ is negligible, thus verifying the overall accuracy of the present measurements. Similar, but less detailed attempts to determine the budget of $\frac{1}{2}\overline{\theta^2}$ were made by Antonia, Danh & Prabhu (1977) and Verollet (1972) [see also Fulachier *et al.* 1982]. Although Antonia *et al.* (1977) obtained

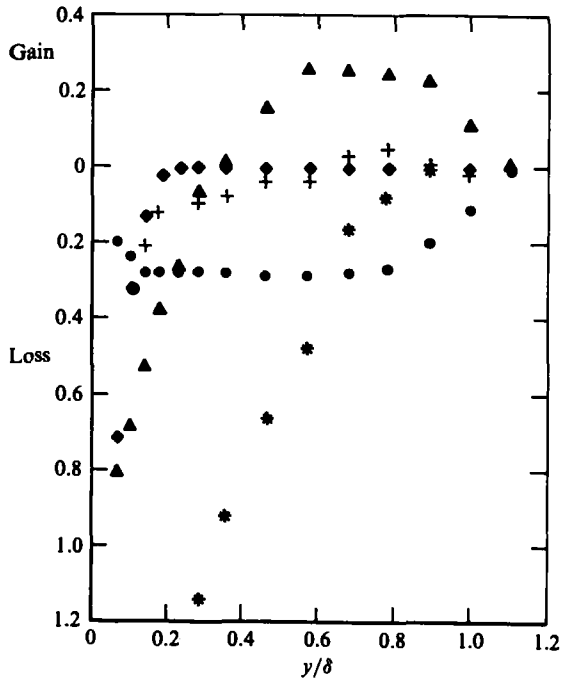

FIGURE 7. Diffusion, advection and imbalance of $\frac{1}{2}\overline{\theta^2}$ in the outer layer. All terms are normalized by $(\delta/U_\tau\theta_\tau^2)$. Note that the vertical scale is larger than that of figure 6 by a factor 20. ▲, turbulent diffusion; ●, advection; ◆, molecular gradient diffusion; +, imbalance for total dissipation; *, imbalance for isotropic dissipation.

a satisfactory closure of the budget at their last measurement location, they approximated the dissipation with $3\alpha(\overline{\theta^2}_{,x}+\overline{\theta^2}_{,y})$. The present measurements indicate that this approximation underestimates $\bar{\epsilon}_\theta$ by about 10 % for $y/\delta > 0.25$. In Verollet's case, the diffusion was not measured but inferred by difference. It is difficult to assess the accuracy of this diffusion by checking the approximation

$$\int_0^\delta \left(\frac{\partial(\overline{v\theta^2})}{\partial y}\right) \mathrm{d}y \approx 0, \tag{10}$$

since the magnitude $\partial(\overline{v\theta^2})/\partial y$ is very small for $y^+ \gtrsim 40$, and Verollet's measurements fall in this region. Relatively large values of $\partial(\overline{v\theta^2}/\partial y)$ occur in the region $y^+ \lesssim 40$. Since the gain and loss, due to diffusion, are approximately in balance in the outer layer, one expects the gain of $\overline{\theta^2}$, due to turbulent diffusion, in the region $y^+ \lesssim 40$ to be approximately equal to the loss of $\overline{\theta^2}$ due to turbulent diffusion. Checking (10) would therefore amount to checking the approximation

$$\int_0^{y^+\approx 40} \frac{\partial}{\partial y^+}(\overline{v^+\theta^{+2}})\,\mathrm{d}y^+ \approx 0. \tag{11}$$

The extent by which (11) is satisfied represents either a measure of the accuracy, in the near-wall region, of $\overline{v^+\theta^{+2}}$ when the latter is measured directly or an indirect measure of the accuracy of other terms in the near-wall budget when $\overline{v^+\theta^{+2}}$ is inferred by difference. The extent by which (11) is satisfied by the present budget is discussed in §6.

For $y/\delta < 0.25$, the imbalance, for the present budget, increases slightly due to the

increased uncertainties in the measurements of production, diffusion and, in particular, dissipation. The imbalance that would have existed if isotropy had been used to determine $\bar{\epsilon}_\theta$ is shown in figures 6 and 7. This imbalance is as large as the magnitude of the isotropic dissipation for $0.07 < y/\delta < 0.2$, reflecting the increasing anisotropy as the wall is approached.

6. Behaviour of the budget close to the wall

The satisfactory closure of the budget of $\frac{1}{2}\overline{\theta^2}$ in the outer layer, achieved with all three measured components of $\bar{\epsilon}_\theta$, was sufficiently encouraging to attempt the construction of the budget in the near-wall region. This construction would enable the turbulent diffusion to be inferred by difference. In this region, the first, second, third, fifth and seventh terms of (9) can be neglected by using the boundary-layer approximation. The remaining terms can be made dimensionless by multiplying with $\nu/u_\tau^2\theta_\tau^2$ and written in the form

$$\underset{\text{production I}}{\overline{v^+\theta^+}\frac{\partial\overline{T}^+}{\partial y^+}} + \underset{\text{turbulent diffusion II}}{\frac{1}{2}\frac{\partial(\overline{v^+\theta^{+2}})}{\partial y^+}} - \underset{\text{molecular diffusion III}}{\frac{1}{2Pr}\frac{\partial^2(\overline{\theta^{+2}})}{\partial y^{+2}}} + \underset{\text{dissipation IV}}{\frac{\nu}{u_\tau^2\theta_\tau^2}\bar{\epsilon}_\theta} = 0, \tag{12}$$

where Pr is the molecular Prandtl number ($= \nu/\alpha$). Direct estimates† of I and II in the near-wall region are precluded in the present study due to the size of the X-wire/cold-wire arrangement. To calculate I, $\overline{v\theta}$ was obtained by numerically integrating the mean enthalpy equation

$$\bar{U}\frac{\partial\bar{T}}{\partial x} + \bar{V}\frac{\partial\bar{T}}{\partial y} = \alpha\frac{\partial^2\bar{T}}{\partial y^2} - \frac{\partial}{\partial y}(\overline{v\theta}). \tag{13}$$

The behaviour of $\overline{v\theta}$ and $\bar{T}$ in the near-wall region can be obtained from the Taylor series expansion of mean and fluctuating components of velocity and temperature. Using the no-slip condition at the wall and the continuity equations for mean and fluctuating quantities, expressions for the components of term I can be written as (e.g. Antonia 1980)

$$\overline{v^+\theta^+} = \alpha_3 y^{+3} + \alpha_4 y^{+4} + O(y^{+5}), \tag{14}$$

$$\overline{T}^+ = Pr\, y^+ + \beta_3 y^{+4} + \beta_4 y^{+5} + O(y^{+6}), \tag{15}$$

where the coefficients α_3, α_4, β_3 and β_4 may depend on Pr. The constants α_3 and α_4 can be related to β_3 and β_4 if the contribution from the left-hand side of (13) is assumed to be zero, which is equivalent to assuming that the total heat flux is constant, viz.

$$Q_w = \overline{v\theta} - \alpha\frac{\partial\bar{T}}{\partial y} = \text{constant}. \tag{16}$$

The values for β_3 and β_4 were obtained from least-squares regressions of (15) to measurements of $\overline{T}^+$ in the range $1 \leqslant y^+ \leqslant 10$. Average values of -1.78×10^{-4} and 7.4×10^{-6} were obtained for β_3 and β_4 respectively. By comparison, Antonia (1980) obtained values of -1.4×10^{-4} and 5.6×10^{-6} using Blom's (1970) measurements. The production term I (figure 8) in the region $y^+ < 15$, estimated from a distribution of $\overline{v\theta}$ calculated with (13) agrees to within 1 % with the estimate obtained by using

† Nagano & Hishida (1985) obtained I and II directly using a specially designed three-wire probe permitting near-wall measurements of v.

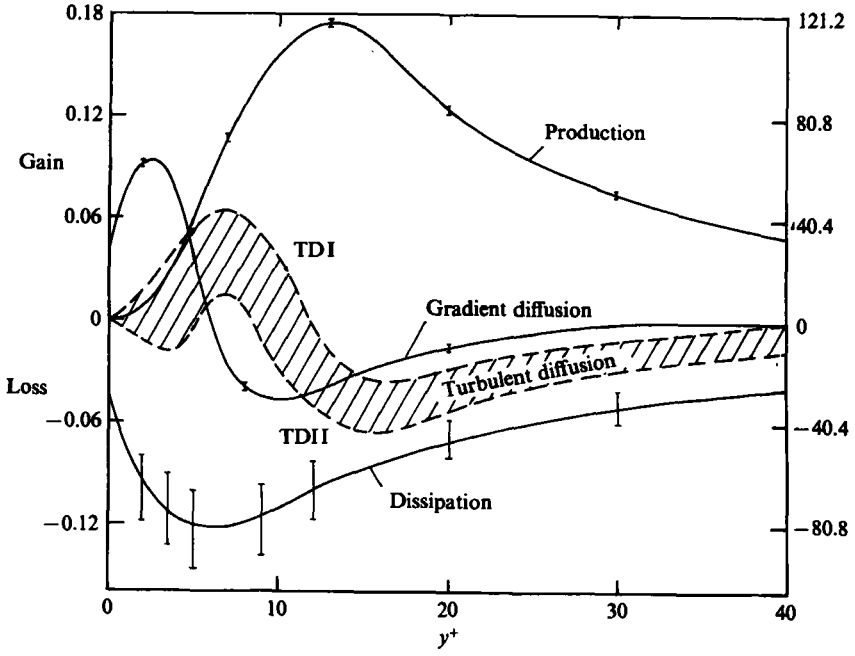

FIGURE 8. Budget of $\frac{1}{2}\overline{\theta^2}$ in the near-wall region. Hatched area is an estimate of the experimental uncertainty for the turbulent diffusion. All terms are normalized by $(\nu/u_\tau^2\theta_\tau^2)$. Numbers on the left-hand side of the ordinate correspond to the normalization with $(\delta/u_\tau\theta_\tau^2)$.

(14) and (15) and assumption (16). It was encouraging to note that the measured production at $y^+ = 50$ agrees to within 8% with the value calculated with (13).

At the wall, (9) satisfies the following condition

$$\frac{\alpha}{\nu}\overline{\left(\frac{\partial\theta^+}{\partial y^+}\right)^2} = \frac{\alpha}{2\nu}\frac{\partial^2\overline{\theta^{+2}}}{\partial y^{+2}}, \tag{17}$$

representing an equality between the dissipation and the molecular diffusion, permitting the estimation of dissipation at the wall. This result also follows from the identity

$$\frac{\partial^2\theta^{+2}}{\partial y^{+2}} = 2\left(\frac{\partial\theta^+}{\partial y^+}\right)^2, \tag{18}$$

valid at $y^+ = 0$. The contribution of the molecular diffusion to the budget is confined only to the region close to the wall ($y^+ \leqslant 30$). The molecular diffusion plotted in figure 8 was obtained by numerically differentiating the cubic-spline least-squares fit to the measurements of $\overline{\theta^{+2}}$. The maximum in the molecular diffusion occurs at $y^+ \approx 2.5$. Interestingly, the maximum in the corresponding term of the near-wall turbulent-energy budget also occurs at $y^+ \approx 2.5$ (Bernard & Berger 1984). It is also important to note that the resulting value of $\frac{1}{2}(\partial^2\overline{\theta^{+2}}/\partial y^{+2})$ at $y^+ = 0$ is consistent with the measured values of $\overline{(\partial\theta^+/\partial y^+)^2}$ at $y^+ \leqslant 5$.

The turbulent diffusion was inferred by difference. The shaded region in figure 8 is our estimate of the error in the turbulent diffusion, the upper (TD1) and lower (TD2) bounds of this region corresponding to the lower and upper limits respectively of the range of the dissipation measurements. The distribution TD1 satisfies approximation (11) closely, the gain of $\frac{1}{2}\overline{\theta^2}$ representing about 95% of the loss. On this basis, TD1 is a plausible distribution for the turbulent diffusion in the near-wall

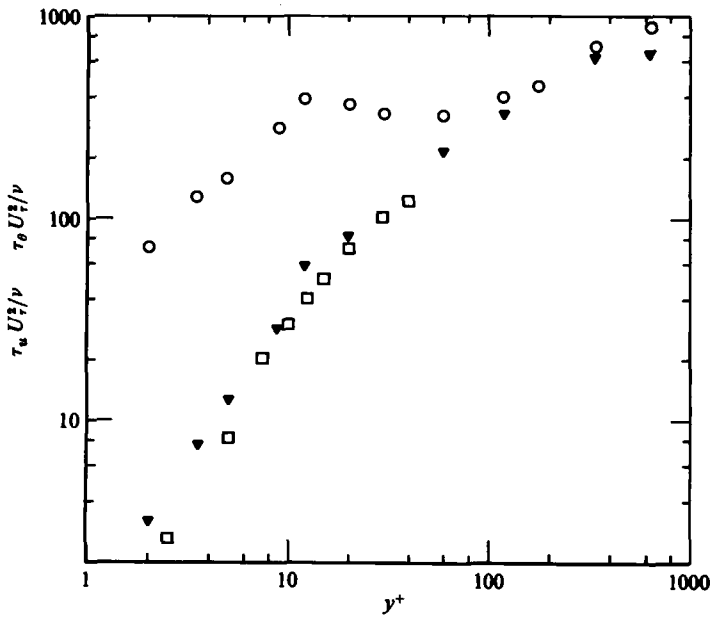

FIGURE 9. Dissipation timescales of velocity and temperature. ▼, τ_θ; ○, τ'_θ; □, τ_u (from the data of Laufer 1954).

region. This distribution compares well with that measured by Nagano & Hishida (1985) for $y^+ \gtrsim 12$, both distributions indicating a loss of $\frac{1}{2}\overline{\theta^2}$ due to turbulent diffusion. For $y^+ < 12$, Nagano & Hishida's (1985) measurements indicate a gain in diffusion, as inferred in our study. However, the magnitude of this gain is insufficient to satisfy relation (11).

7. Temperature timescale

The variation, across the boundary layer, of the temperature-dissipation timescale $\tau_\theta (\equiv \overline{\theta^2}/\bar{\epsilon}_\theta)$ estimated from measurements of $\overline{\theta^2}$ and of the totall dissipation $\bar{\epsilon}_\theta$, is shown in figure 9. Also shown are estimates of $\tau'_\theta \equiv \overline{\theta^2}/(\bar{\epsilon}_\theta)_{\rm iso}$, calculated from measurements of $\overline{\theta^2}$ and the isotropic dissipation $(\bar{\epsilon}_\theta)_{\rm iso}$. Whereas τ_θ increases nearly continuously across the layer, τ'_θ is approximately constant in the region $10 \lesssim y^+ \lesssim 100$. In the near-wall region, τ'_θ is larger than τ_θ by a factor of about 10. Although the difference between τ'_θ and τ_θ is smaller in the outer region, this difference is probably sufficiently important to be taken into account when modelling this region of the flow.

Although the complete determination of the turbulent-energy dissipation $\bar{\epsilon}$ is considerably more involved than that of $\bar{\epsilon}_\theta$, it seemed useful to establish the relationship between τ_θ and the corresponding timescale τ_u $(\equiv \overline{q^2}/\bar{\epsilon})$ for the velocity field. Although it has been established (Launder 1976) that the prescription $R = \tau_\theta/\tau_u =$ constant is neither sufficiently general nor reliable for inferring $\bar{\epsilon}_\theta$, once $\overline{q^2}$, $\overline{\theta^2}$ and $\bar{\epsilon}$ are known, our enquiry into the magnitude of the ratio R in the near-wall region is important in view of the similarity between the momentum and thermal fields in this region and because of the possibility of substituting τ_θ for τ_u in models of transport equations for the Reynolds stresses. To this end, we have calculated τ_u from Laufer's (1954) measurements of $\overline{q^2}$ and $\bar{\epsilon}$ in the near-wall region of a fully developed pipe flow. Laufer measured five of the nine major terms of $\bar{\epsilon}$, and assumed

isotropy to estimate the remaining four terms. Townsend (1956) corrected Laufer's measurements for the effect of the gradient of $\overline{u^2}$ close to the wall. These corrected values of $\bar{\epsilon}$ have been used in our estimate of τ_u. The distribution of τ_u has only been obtained up to $y^+ \approx 40$ (figure 9). The scales τ_θ and τ_u are nearly equal and therefore R is nearly unity in this region. The experimental uncertainty associated with this ratio would reflect primarily the uncertainty of determining $\bar{\epsilon}$ and, to a lesser degree, the uncertainties in $\overline{q^2}$ and $\overline{\theta^2}$. Substituting Kreplin & Eckelmann's (1979) near-wall values of $\overline{q^2}$ for those of Laufer did not affect the distribution of τ_u.

Nagano & Hishida (1985) obtained a nearly uniform value of 0.5 for R in the near-wall region. This small value of R may be due to a possible overestimation of the temperature dissipation which was obtained by difference in their study. As noted earlier, Nagano & Hishida's measurements of diffusion appear to be too small close to the wall; an increase in the magnitude of this diffusion term would result in a decrease in $\bar{\epsilon}_\theta$ and an increase in the value of R.

8. Concluding remarks

The three components of the temperature dissipation have been estimated from the temporal temperature derivative using Taylor's hypothesis and from the curvature of the two-point temperature autocorrelations in the y- and z-directions. In the outer layer ($y/\delta \gtrsim 0.25$), the magnitude of the components of $\bar{\epsilon}_\theta$ are such that $\overline{\theta^2}_{,z} > \overline{\theta^2}_{,y} > \overline{\theta^2}_{,x}$ and the average values for the ratios $\overline{\theta^2}_{,y}/\overline{\theta^2}_{,x}$ and $\overline{\theta^2}_{,z}/\overline{\theta^2}_{,x}$ are about 1.4 and 1.6 respectively. Although these values are based on only a limited amount of data (four points for $y/\delta \gtrsim 0.25$), they support previous results by Sreenivasan *et al.* (1977). The negligible imbalance for the budget of $\frac{1}{2}\overline{\theta^2}$ in the outer layer suggests that the temperature dissipation has been measured with good accuracy in that region.

In the near-wall region, which is the main region of interest of this study, the relative magnitudes of the components of $\bar{\epsilon}_\theta$ underscore the increased departure from isotropy as the wall is approached. For example, the ratio of the total dissipation to the isotropic dissipation increases from about 2 at $y^+ = 40$ to a value as large as 30 at $y^+ = 2$. Although the uncertainty band associated with the turbulent diffusion, obtained by difference, is relatively large, (11) is closely satisfied by the upper bound of our diffusion estimates. This gives an indirect but encouraging indication of the correctness of the $\bar{\epsilon}_\theta$ data. It would of course be desirable to measure the turbulent diffusion in the near-wall region. Such a measurement would necessitate the normal velocity fluctuation v to be obtained simultaneously with the temperature fluctuation. It is possible that a miniaturized version of the three-parallel-wire probe of Rey & Béguier (1977) can be used for this purpose.

Molecular diffusion is comparable in magnitude to the turbulent diffusion in the near-wall region and becomes negligible only beyond $y^+ \approx 30$. The limiting behaviour, as $y^+ \to 0$, of the instantaneous temperature equation requires that the molecular diffusion balances the dissipation at the wall.

The present measurements of $\bar{\epsilon}_\theta$ have enabled the temperature dissipation timescale to be estimated in the near-wall region. These estimates should be useful when, as the present computational trends indicate, the current wall-function treatment is replaced by a direct simulation of the transport equations in the near-wall region. In view of the close similarity observed (e.g. the flow visualization of Iritani *et al.* 1985) between the velocity and thermal fields in the near-wall region, it is possible that the temperature-dissipation timescale can be used to model not only the

temperature–pressure gradient terms in the heat-flux transport equations but also the pressure–rate-of-strain terms in the Reynolds-stress transport equations. The present results give $R \approx 1$ and provide reasonable support for the use of the temperature-dissipation timescale in second-order models for the near-wall region.

The support of the Australian Research Grants Scheme is gratefully acknowledged.

REFERENCES

ANTONIA, R. A. 1980 *Intl J. Heat Mass Transfer*, **23**, 906.

ANTONIA, R. A. & BROWNE, L. W. B. 1983 *J. Fluid Mech.* **134**, 67.

ANTONIA, R. A., BROWNE, L. W. B., BRITZ, D. & CHAMBERS, A. J. 1984 *Phys. Fluids* **27**, 87.

ANTONIA, R. A., DANH, H. Q. & PRABHU, A. 1977 *J. Fluid Mech.* **80**, 153.

ANTONIA, R. A., SATYAPRAKASH, B. R. & HUSSAIN, A. K. M. F. 1980 *Phys. Fluids* **23**, 695.

BERNARD, P. S. & BERGER, B. S. 1984 *AIAA J.* **22**, 306.

BLOM, J. 1970 Ph.D. thesis, Technological University, Eindhoven.

BROWNE, L. W. B., ANTONIA, R. A. & CHAMBERS, A. J. 1983*a* *Boundary-Layer Met.* **27**, 129.

BROWNE, L. W. B., ANTONIA, R. A. & RAJAGOPALAN, S. 1983*b* *Phys. Fluids* **26**, 1222.

CANTWELL, B. J. 1981 *Ann. Rev. Fluid Mech.* **13**, 457.

CORRSIN, S. 1953 *Proc. 1st Iowa Symp. on Thermodynamics, State University of Iowa*, p. 5.

FULACHIER, L., ELENA, M., VEROLLET, E. & DUMAS, R. 1982 In *Structure of Turbulence in Heat and Mass Transfer* (ed. Z. P. Zaric), p. 193. Hemisphere.

HINZE, O. 1959 *Turbulence: Introduction to its Mechanism and Theory.* McGraw-Hill.

IRITANI, Y., KASAGI, N. & HIRATA, M. 1985 In *Turbulent Shear Flows* (ed. L. J. S. Bradbury, F. Durst, B. E. Launder, F. W. Schmidt & J. H. Whitelaw), vol. 4, p. 223. Springer.

KLEBANOFF, P. S. 1954 *NACA Rep.* TN-1247.

KREPLIN, H. P. & ECKELMANN, H. 1979 *Phys. Fluids* **22**, 1233.

LAUFER, J. 1954 *NACA Rep.* TR-1174.

LAUNDER, B. E. 1976 *Topics in Applied Physics* **12**, 231.

LAUNDER, B. E. 1984 *Intl J. Heat Mass Transfer* **27**, 1485.

LAUNDER, B. E. & SPALDING, D. B. 1974 *Comp. Meth. Appl. Mech. Engng.* **3**, 269.

LECORDIER, J. C., DUPONT, A., GAJAN, P. & PARANTHOEN, P. 1984 *J. Phys.* E: *Sci. Instrum.* **17**, 307.

MESTAYER, P. & CHAMBAUD, P. 1979 *Boundary-Layer Met.* **16**, 311.

NAGANO, Y. & HISHIDA, M. 1985 *Proc. Fifth Turbulent Shear Flow Conference, Cornell University*, p. 1419.

REY, C. & BÉGUIER, C. 1977 *DISA Information* **21**, 11.

ROSE, W. G. 1966 *J. Fluid Mech.* **25**, 97.

SHIH, T.-H. & LUMLEY, J. L. 1986 *Phys. Fluids* **29**, 971.

SMITH, C. R. & METZLER, S. P. 1983 *J. Fluid Mech.* **129**, 27.

SREENIVASAN, K. R., ANTONIA, R. A. & DANH, H. Q. 1977 *Phys. Fluids* **20**, 1238.

TENNEKES, H. & LUMLEY, J. L. 1972 *A First Course in Turbulence.* MIT Press.

TOWNSEND, A. A. 1956 *The Structure of Turbulent Shear Flow*, 1st ed. Cambridge University Press.

VEROLLET, E. 1972 Ph.D. thesis, Université d'Aix-Marseille II (also *Rapport* CEA-R-4872, CEN, Saclay, 1977).

WYNGAARD, J. C. 1971 *J. Fluid Mech.* **48**, 763.